

1 **Title:** A bright and high-performance genetically encoded Ca^{2+} indicator
2 based on mNeonGreen fluorescent protein

3
4 **Authors:** Landon Zarowny¹ (equal contribution), Abhi Aggarwal^{1,2} (equal contribution),
5 Virginia M.S. Rutten^{2,3}, Ilya Kolb², The GENIE Project², Ronak Patel², Hsin-Yi Huang⁴, Yu-Fen
6 Chang⁴, Tiffany Phan¹, Richard Kanyo⁵, Misha Ahrens², W. Ted Allison⁵, Kaspar Podgorski²,
7 Robert E. Campbell^{1,6}

8 **Affiliations**

9 ¹Department of Chemistry, University of Alberta, Edmonton, Alberta, Canada

10 ²Janelia Research Campus, Howard Hughes Medical Institute, Ashburn, Virginia, United States

11 ³Gatsby Computational Neuroscience Unit, UCL, London, UK

12 ⁴LumiSTAR Biotechnology, Inc. National Biotechnology Research Park, Taipei City 115, Taiwan

13 ⁵Department of Biological Sciences, University of Alberta, Edmonton, Alberta, Canada

14 ⁶Department of Chemistry, Graduate School of Science, The University of Tokyo, Tokyo, Japan

15

16 **Abstract**

17 Genetically encodable calcium ion (Ca^{2+}) indicators (GECIs) based on green fluorescent
18 proteins (GFP) are powerful tools for imaging of cell signaling and neural activity in model
19 organisms. Following almost two decades of steady improvements in the *Aequorea victoria* GFP
20 (avGFP)-based GCaMP series of GECIs, the performance of the most recent generation (i.e.,
21 GCaMP7) may have reached its practical limit due to the inherent properties of GFP. In an effort
22 to sustain the steady progression towards ever-improved GECIs, we undertook the
23 development of a new GECI based on the bright monomeric GFP, mNeonGreen (mNG). The
24 resulting indicator, mNG-GECO1, is 60% brighter than GCaMP6s *in vitro* and provides
25 comparable performance as demonstrated by imaging Ca^{2+} dynamics in cultured cells, primary
26 neurons, and *in vivo* in larval zebrafish. These results suggest that mNG-GECO1 is a promising

27 next-generation GECI that could inherit the mantle of GCaMP and allow the steady
28 improvement of GECIs to continue for generations to come.

29 Introduction

30 Genetically encodable calcium ion (Ca^{2+}) indicators (GECIs) are a class of single fluorescent
31 protein (FP)-based biosensors that are powerful tools for the visualization of Ca^{2+} concentration
32 dynamics both *in vitro* and *in vivo*^{1, 2, 3}. As they are genetically encoded, GECI expression can
33 be genetically targeted to specific cell types or subcellularly localized to specific organelles.
34 Furthermore, their negligible cellular toxicity, minimal perturbation of endogenous cellular
35 functions, and biological turnover, make them ideal for long-term imaging experiments⁴. The
36 Ca^{2+} -dependent fluorescent response of GECIs is routinely used as a proxy for neuronal activity
37 due to the transient changes in Ca^{2+} concentration that accompany action potentials^{5, 6, 7, 8}.
38 GECIs have facilitated the optical recording of thousands of neurons simultaneously in the
39 surgically exposed brains of mice⁹. Despite their widespread use by the scientific community,
40 there are some properties of GECIs that could be further improved. These properties include
41 faster Ca^{2+} response kinetics, higher fluorescent molecular brightness, and minimized
42 contribution to Ca^{2+} buffering. Some GECIs have shown aggregation in neurons, and some of
43 the most highly optimized GECIs have been demonstrated to cause aberrant cortical activity in
44 murine models^{10, 11, 12}.

45 An important issue that is common to all GECIs is their intrinsic Ca^{2+} buffering capacity.
46 The Ca^{2+} binding domains of GECIs (calmodulin (CaM) or troponin C (TnC)) act as Ca^{2+} buffers
47 within the cell and must necessarily compete with endogenous proteins for binding to Ca^{2+}
48 (Refs. 13, 14, 15, 16). Comprehensive investigations of this phenomenon are limited, but a few
49 reports have indicated abnormal morphology and behavior of neurons after long term or high
50 expression of GCaMPs¹⁷. Ca^{2+} buffering and competition for CaM binding sites have been
51 proposed as possible causes. One solution to the Ca^{2+} buffering phenomenon is to reduce the
52 reporter protein expression, leading to a lower concentration of GECI and reduced buffering
53 capacity. However, reduced expression requires increased intensity of excitation light to achieve
54 an equivalent fluorescent signal, which can lead to increased phototoxicity and photobleaching.
55 Another solution is to reduce the number of Ca^{2+} binding sites like that in the TnC-based GECIs,
56 NTnC¹⁸ and YTnC¹⁹. Unfortunately, these indicators have relatively low fluorescence response
57 ($\Delta F/F_{\min} \sim 1$ for NTnC and ~ 10.6 for YTnC) compared to the recent GCaMP7 variants ($\Delta F/F_{\min} \sim$
58 21 to 145)²⁰. Another possible solution is to develop GECIs with increased brightness such that

59 they could be expressed at a lower concentration while retaining a similar fluorescent intensity
60 with similar intensity of excitation light.

61 Further increasing the brightness of GECIs, while retaining high performance
62 comparable to the most recent generation of indicators, would provide improved tools for optical
63 imaging of neuronal activity and decrease the occurrence of experimental artifacts resulting
64 from Ca^{2+} buffering and indicator overexpression¹⁷. Our efforts to realize this advance were
65 inspired, in part, by the advent of a bright and monomeric engineered version of GFP from
66 *Branchiostoma lanceolatum*, mNeonGreen (mNG)²¹. Due to its high brightness and its excellent
67 performance as a subcellular localization tag²¹, mNG is an exceptionally promising starting point
68 from which to develop a brighter GECI.

69 Here we introduce an mNG-based genetically encodable Ca²⁺ indicator for optical
70 imaging (mNG-GECO1) that exceeds the brightness of all variants in the GCaMP series while
71 providing performance that is comparable to the latest generation GCaMP variants. Key design
72 differences between mNG-GECO1 and the GCaMP series include the GFP portion (mNG
73 versus avGFP) and the protein topology (non-circularly permuted mNG versus circularly
74 permuted avGFP).

75

76 **Results and Discussion**

77 **Rational engineering and iterative directed evolution of mNG-GECO1**

78 We used a combination of rational design, linker sequence optimization, and directed evolution
79 to develop mNG-GECO1 (**Supplementary Fig. 1**). Starting from an unpublished topological
80 variant of REX-GECO1²², we used PCR to produce a fragment containing CaM linked to the
81 RS20 peptide with a short linker (**Fig. 1a**). Insertion of this PCR fragment into the mNG gene
82 between residues 136 and 137 (numbering as in PDB ID 5LTR)²³ resulted in a green fluorescent
83 indicator prototype which we named mNG-GECO0.1 (**Fig. 1**). For the remainder of this
84 manuscript, amino acids will be numbered as in the sequence alignment provided as
85 **Supplementary Fig. 2**. mNG-GECO0.1 had a minimal response to Ca^{2+} ($\Delta F/F_{\min} = 0.3$), but we
86 anticipated that optimization of the sequence around the insertion site would yield a suitable
87 template for directed evolution. Indeed, we found that deletion of Ala146, the residue

88 immediately preceding the insertion of the Ca²⁺ sensing domain, substantially improved the
89 response to Ca²⁺ (mNG-GECO0.2; $\Delta F/F_{\min} \sim 2$).

90 Starting from mNG-GECO0.2, we began a process of iterative directed evolution which
91 involved screening of libraries created from error-prone PCR or site saturation mutagenesis to
92 identify variants with increased brightness and increased response to Ca²⁺. In our primary
93 library screen, we used a fluorescent colony screening system equipped with excitation and
94 emission filters appropriate for imaging of green fluorescence²⁴. Bright colonies were picked and
95 cultured overnight in liquid media. A secondary screen for Ca²⁺ sensitivity was performed the
96 next day using detergent-extracted bacterial lysate. The fluorescence of the lysate for each
97 variant was measured in Ca²⁺ chelating buffer (30 mM MOPS, 100 mM KCl, 10 mM EGTA, pH
98 7.3), and subsequently in Ca²⁺ saturating buffer (30 mM MOPS, 100 mM KCl, 10 mM Ca²⁺, pH
99 7.3). Dividing the Ca²⁺ saturated fluorescence by the Ca²⁺ free fluorescence provided an
100 approximate but robust measure of each indicator variant's response to Ca²⁺. For each round of
101 screening the plasmids were isolated for the 6-10 most promising variants and sent for
102 sequencing. The pool of these most promising variants was used as the template for the next
103 round of library creation and directed evolution.

104 Following 7 rounds of iterative directed evolution, *E. coli* colonies harboring mNG-
105 GECO0.7 were brightly fluorescent after overnight incubation. However, the Ca²⁺ response of
106 mNG-GECO0.7 was remained relatively low ($\Delta F/F_{\min} \sim 5$), relative to recent generation GCaMP
107 variants. We anticipated that optimization of the linkers connecting mNG to the CaM-RS20
108 domain (mNG-CaM linker and RS20-mNG linker) could lead to the identification of variants with
109 improved responses. To optimize these linker regions, we used site saturation mutagenesis to
110 produce libraries of all 20 amino acids within the 3 residues connecting mNG to CaM. Individual
111 libraries of Leu133, Thr134, and Ala135 were randomized to all 20 amino acids. If a beneficial
112 mutation was found, the process was repeated for the remaining amino acids until these
113 libraries were exhausted. By screening of these libraries, we identified two mutations of the
114 linker region between mNG barrel and CaM: Ala145Gly and Leu143Ile. This variant, mNG-
115 GECO0.9, had a $\Delta F/F_{\min} \sim 12$ as measured *in vitro*.

116 Following optimization of the mNG-CaM linker, multiple site saturation libraries were
117 created, using the same methodology as the mNG-CaM linker, for the RS20-mNG linker region
118 (residues Glu323, Trp324, Cys325 and Arg326). Screening of these libraries led to the
119 identification of a particularly bright variant with a Cys325Asn mutation. This variant, designated

120 mNG-GECO0.9.1, is brighter than mNG-GECO0.9 but has a decreased response to Ca^{2+} of
121 $\Delta F/F_{\min} = 3.5$. In an effort to improve the performance of mNG-GECO0.9.1, we applied site
122 saturations to positions previously found to be mutated during directed evolution. Screening of
123 these libraries for variants with increased brightness and higher $\Delta F/F_{\min}$ led to the identification
124 of a variant with Asp206Gly, Phe209Leu, Pro263Phe, Lys265Ser, Thr346Ile and the reversion
125 of Gly152Glu. This variant was designated as mNG-GECO1. A notable observation from the
126 directed evolution efforts is the minimal number of mutations in the mNG domain. Only 2
127 mutations (Lys128Glu and Thr346Ile) were outside the β -strand in which the Ca^{2+} sensing
128 domain was inserted. In contrast, 3 mutations were localized to the β -strand surrounding the
129 sensing domain insertion site (Leu143Ile/Ala145Gly/Cys325Asn) and 7 mutations were localized
130 to the CaM domain
131 (Thr151Ala/Thr180Cys/Asp206Gly/Phe209Leu/Pro263Phe/Lys265Ser/Ala293Gly).

132 ***In vitro* characterization of mNG-GECO1**

133 We characterized mNG-GECO1, in parallel with GCaMP6s, for direct comparison of biophysical
134 properties measured under identical conditions (**Supplementary Table 1**). We found that the
135 excitation (ex) and emission (em) maxima of the Ca^{2+} saturated states to be 497 nm (ex) and
136 512 nm (em) for GCaMP6s and 496 nm (ex) and 513 nm (em) for mNG-GECO1 (**Fig. 1**). The *in*
137 *vitro* Ca^{2+} response of mNG-GECO1 ($\Delta F/F_{\min} = 35$) was similar to that of GCaMP6s when tested
138 in parallel ($\Delta F/F_{\min} = 39$). The K_d of mNG-GECO1 (810 nM) is substantially higher than that of
139 GCaMP6s (147 nM). This increase in K_d is consistent with the faster k_{off} kinetics of mNG-
140 GECO1 ($k_{\text{off}} = 1.57 \pm 0.01 \text{ s}^{-1}$) relative to GCaMP6s ($k_{\text{off}} = 1.06 \pm 0.01 \text{ s}^{-1}$). There was no
141 noticeable difference observed between the k_{on} kinetics of mNG-GECO1 and GCaMP6s with
142 varying concentrations of Ca^{2+} (**Supplementary Fig. 3**).

143 In the Ca^{2+} bound state, mNG-GECO1 has an extinction coefficient of $102,000 \text{ M}^{-1} \text{ cm}^{-1}$
144 and quantum yield of 0.69, giving it an overall brightness (= EC * QY) of 70. This value is similar
145 to the value of 77 previously reported for NTnC¹⁸ and 78% of the brightness of mNG itself
146 (measured by us to be $112,000 \text{ M}^{-1} \text{ cm}^{-1} * 0.8 = 90$) (**Supplementary Fig. 4**). Under two-photon
147 excitation conditions, both mNG-GECO1 and GCaMP6s have a maximal two-photon cross
148 section at $\sim 970 \text{ nm}$ and similar action cross-section (AXS) values of 37.22 GM for mNG-
149 GECO1 and 38.81 GM for GCaMP6s. However, due to its higher brightness at the single
150 molecule level, the molecular brightness of mNG-GECO1 (21.3) is higher than that of GCaMP6s

151 (16.1) at 15 mW power. Overall, these data indicate the mNG-GECO1 has excellent one-photon
152 and two-photon excitation properties *in vitro*.

153

154 **In vitro characterization in cultured cells and dissociated neurons**

155 To compare the performance of mNG-GECO1 and GCaMP6s in cultured cells, we transfected
156 HeLa cells with mNG-GECO1 in a pcDNA vector (CMV promoter) in parallel with pGP-CMV-
157 GCaMP6s. Using a previously reported protocol²⁵, Ca²⁺ oscillations were induced by treatment
158 with histamine and fluorescence images were acquired every 10 seconds for 20 minutes. From
159 the intensity versus time data for each cell, $\Delta F/F_0$ for all oscillations of $\Delta F/F_0 > 0.5$ were
160 extracted using a Matlab script. Using these extracted $\Delta F/F_0$ values, average $\Delta F/F_0$ for all
161 oscillations and maximum $\Delta F/F_0$, was computed. The average maximum $\Delta F/F_0$ was calculated
162 by averaging the maximum $\Delta F/F_0$ from each responding cell. In parallel experiments, mNG-
163 GECO1 had an average $\Delta F/F_0 = 4.50 \pm 2.96$ compared to GCaMP6s' $\Delta F/F_0 = 3.48 \pm 2.40$ (**Fig.**
164 **1h**). The maximum $\Delta F/F_0$ was 16.8 ± 10.5 for mNG-GECO1 and 12.8 ± 6.11 for GCaMP6s. At
165 the end of the 20-minute imaging experiment, the cells were treated with ionomycin/Ca²⁺ to
166 saturate the indicators and induce a fluorescent maximum and then with Ca²⁺ chelator
167 EGTA/ionomycin to deplete Ca²⁺ and produce a fluorescent minimum. For these treatments,
168 $\Delta F/F_{\min} = 48.8 \pm 15.1$ for mNG-GECO1 and $\Delta F/F_{\min} = 16.7 \pm 5.2$ for GCaMP6s. These results
169 were obtained from a data set of 137 responding cells with 1624 individual oscillations for mNG-
170 GECO1 and 99 responding cells with 687 individual oscillations for GCaMP6s (**Supplementary**
171 **Table 2**).

172 We next characterized the performance of mNG-GECO1 in dissociated rat cortical
173 neurons alongside GCaMP series indicators GCaMP6s, jGCaMP7s, jGCaMP7b, jGCaMP7c,
174 and jGCaMP7f (**Fig. 2**). Field stimulated neurons expressing mNG-GECO1 had a single action
175 potential (AP) $\Delta F/F_0 = 0.19 \pm 0.04$, slightly lower than that of GCaMP6s ($\Delta F/F_0 = 0.27 \pm 0.09$,
176 **Fig. 2a**). For 10 APs, performance of mNG-GECO1 was approximately twofold lower than
177 GCaMP6s, with $\Delta F/F_0$ of 1.5 ± 0.19 and 3.1 ± 0.26 for mNG-GECO1 and GCaMP6s,
178 respectively (**Fig. 2b**). At 160 APs, mNG-GECO1 has a $\Delta F/F_0$ of 6.5 ± 0.8 , slightly lower than
179 GCaMP6s's $\Delta F/F_0$ of 9.0 ± 0.47 (**Fig. 2c**). The baseline brightness of mNG-GECO1 ($1,374 \pm 31$
180 AU) was comparable to the baseline brightness of GCaMP6s ($1,302 \pm 6$ AU) and jGCaMP7s
181 ($1,397 \pm 11$ AU) (**Fig. 2e**). The signal-to-noise ratio (SNR) of mNG-GECO1 and GCaMP6s are

182 comparable for 1 and 3 AP's (**Fig. 2f**). For 3 AP stimulation, mNG-GECO1 exhibited a half rise
183 time of 49 ± 1 ms and half decay time of 582 ± 12 ms. Under the same conditions, GCaMP6s
184 exhibited a half rise time of 65 ± 2 ms and a half decay time of $1,000 \pm 36$ ms. Field stimulated
185 neuron data is summarized in **Supplementary Table 3**. The overall data in cultured neuron
186 suggest that the mNG-GECO1 sensor is comparable in signal, kinetics, and baseline brightness
187 to the GCaMP6s sensor.

188 ***In vivo* evaluation of mNG-GECO1**

189 To evaluate mNG-GECO1 for *in vivo* expression in zebrafish neurons, we used a Tol2
190 transposase transgenesis system to deliver mNG-GECO1 or GCaMP6s under a pan-neuronal
191 Elavl3 promoter into zebrafish embryos²⁶. We tracked expression of mNG-GECO1 over several
192 days to evaluate the viability of transgenic fish (**Supplementary Fig. 5**). We found no obvious
193 morphological anomalies during larval development stage of zebrafish expressing mNG-GECO1
194 or GCaMP6s.

195 To evaluate the relative performance of mNG-GECO1 and GCaMP6s for imaging of
196 neuronal activity in zebrafish larvae, we used the same transgenesis protocol to produce
197 *Casper* zebrafish lines expressing each indicator (**Fig. 3**). Prior to imaging, 5-6 days post
198 fertilization *Casper* fish expressing the sensors were immobilized with bungarotoxin (1 mg/mL)
199 for 30 seconds followed by a 10 minute incubation in the convulsant 80 mM 4-aminopyridine (4-
200 AP). The fish were then placed in low melting agar and immersed in a solution of 4-AP (80 mM).
201 Imaging consisted of 5 minute intervals of the hindbrain or midbrain at a recording rate of 3 Hz.
202 For each indicator, 5 fish were imaged under 6 different field of views resulting in 834 and 1280
203 individual cells for mNG-GECO1 and GCaMP6s, respectively (**Supplementary Fig. 6**). The
204 resulting data was evaluated using the Suite2p package
205 (<https://github.com/MouseLand/suite2p>)²⁷. We found that mNG-GECO1 had a maximum $\Delta F/F_0$
206 for each cell of 3.09 ± 0.08 compared to 4.56 ± 0.11 for GCaMP6s (**Fig. 3c**). The baseline
207 fluorescence of GCaMP6s was higher compared to mNG-GECO1 (0.95 ± 0.03 vs 1.41 ± 0.05
208 AU, respectively) (**Fig. 3d**). However, the signal-to-noise ratio (SNR), which was computed by
209 dividing the $\Delta F/F_0$ by the raw standard deviation of each cell in six field of views, was higher for
210 mNG-GECO1 (SNR = 6.63 ± 0.07) than GCaMP6s (SNR = 5.25 ± 0.04) (**Fig. 3e**). We also
211 found that mNG-GECO1 had a slower decay time (faster k_{off} kinetics) compared to GCaMP6s
212 (1.98 ± 0.12 s⁻¹ vs 3.00 ± 0.12 s⁻¹, respectively) (**Fig. 3f**). The overall data in zebrafish neurons

213 suggest that mNG-GECO1 is comparable in signal-to-noise ratio, kinetics, and baseline
214 brightness to the GCaMP6s sensor (**Supplementary Table 4**).

215 Ca^{2+} imaging in human iPSC-derived cardiomyocytes

216 Chemical Ca^{2+} dyes such as Fluo-4 acetoxymethyl (AM), Rhod-2 AM and Fura-2 AM are often
217 used to phenotype Ca^{2+} transients in induced pluripotent stem cell-derived cardiomyocytes
218 (iPSC-CM). However, these dyes can be toxic^{28, 29} and may potentially suppress the activity of
219 Na^+ and K^+ -dependent adenosine triphosphatase³⁰. As such, we tested whether mNG-GECO1
220 could serve as a robust tool for observing cells signaling and drug response while preventing
221 cellular toxicity in iPSC-CMs (**Supplementary Fig. 7**). We found that when iPSC-CMs
222 expressing mNG-GECO1 or Fluo-4 AM were treated with 20 mM caffeine, mNG-GECO1 had a
223 2.8 fold higher $\Delta\text{F}/\text{F}$ response than Fluo-4 ($\Delta\text{F}/\text{F} = 11.77 \pm 2.82$ and 4.18 ± 1.27 , respectively)
224 (**Supplementary Fig. 7a, b**). However, when cells were subjected to 0.33 Hz electrical
225 stimulation for 30 minutes, mNG-GECO1 had a slightly lower peak $\Delta\text{F}/\text{F}$ (2.26 ± 0.81) than Fluo-
226 4 AM (3.31 ± 1.42) (**Supplementary Fig. 7c, d**). We suspect that this discrepancy is due to
227 mNG-GECO1's lower affinity for Ca^{2+} . When we stimulated the cells in the presence of 20 mM
228 caffeine, the max $\Delta\text{F}/\text{F}$ of mNG-GECO1 ($\Delta\text{F}/\text{F} = 14.20 \pm 4.67$) was higher than the max $\Delta\text{F}/\text{F}$ of
229 Fluo-4 AM ($\Delta\text{F}/\text{F} = 6.73 \pm 1.19$) (**Supplementary Fig. 7e, f**). Based on this data, we propose
230 that mNG-GECO1 may serve as a useful tool for phenotypic screening and functional tests in
231 iPSC-CMs.

232

233 Conclusion

234 mNG-GECO1 is a new, first-generation, genetically encodable Ca^{2+} indicator that provides
235 performance comparable to 6th and 7th generation GCaMP indicators. We have demonstrated
236 that the *in vitro* performance of mNG-GECO1 in cultured HeLa cells is on par or better than
237 GCaMP6s. However, *in vitro* cultured neuron benchmarking as well as *in vivo* imaging in
238 transgenic zebrafish larvae have indicated that further directed evolution efforts will be required
239 to produce an mNG-GECO1 variant that provides substantial advantages relative to the
240 jGCaMP7 series. Further development of this indicator may come from increasing the Ca^{2+}
241 affinity which would enable more accurate single spike detection. In summary, we have
242 developed a first generation GECl from the mNG scaffold that retains the high fluorescent
243 brightness *in vitro* with performance comparable to the state-of-the-art GECl, GCaMP6s. We

244 expect mNG-GECO1 to be just as amenable to further optimization as the first generation
245 GCaMP, and so mNG-GECO1 is likely to serve as the parent of a new and improved lineage of
246 high performance GECIs.

247 **Author contributions**

248 LZ, AA, and TP performed the directed evolution experiments and *in vitro* characterization. RP
249 performed the *in vitro* 2P characterization, IK and TGP conducted and analyzed the cultured
250 neuron experiments. RK conducted the initial expression experiments of mNG-GECO1 and its
251 variants in zebrafish under the supervision of WTA. VR completed the zebrafish characterization
252 under the supervision of MA. HYH and YFC did the experiments in human iPSC-derived
253 cardiomyocytes. LZ, AA, KP, and REC wrote and edited the manuscript. All authors were
254 allowed to review and edit the manuscript before publication.

255

256 **Acknowledgments**

257 We thank the University of Alberta Molecular Biology Services Unit (Alberta) and Molecular Bio
258 (Janelia) for technical support. We thank Christopher Cairo (Alberta), Andy Holt (Alberta) and
259 Loren Looger (Janelia) for providing access to the instrumentation, Eric Schreiter (Janelia) for
260 providing access to resources and for useful feedback regarding the manuscript. We thank
261 Deepika Walpia (Janelia) and the JRC Histology group for preparing cultured neurons. We
262 thank John Macklin (Janelia) for overseeing two-photon measurements. We thank Nathan
263 Shaner for the mNeonGreen fluorescent protein. REC acknowledges the Japan Society for the
264 Promotion of Science (JSPS), Natural Sciences and Engineering Research Council of Canada
265 (NSERC), and Canadian Institutes of Health Research (CIHR), for funding support. The mNG
266 gene was a kind gift from Jiwu Wang at Allele Biotech.

267

268 **References**

- 269 1. Mank M, Griesbeck O. Genetically encoded calcium indicators. *Chem Rev* **108**, 1550-1564 (2008).
270 2. Akerboom J, *et al.* Optimization of a GCaMP Calcium Indicator for Neural Activity Imaging. *J*
271 *Neurosci* **32**, 13819-13840 (2012).

- 272 3. Knopfel T. Genetically encoded optical indicators for the analysis of neuronal circuits. *Nat Rev*
273 *Neurosci* **13**, 687-700 (2012).
- 274 4. Chen TW, *et al.* Ultrasensitive fluorescent proteins for imaging neuronal activity. *Nature* **499**,
275 295-300 (2013).
- 276 5. Pologruto TA, Yasuda R, Svoboda K. Monitoring neural activity and [Ca²⁺] with genetically
277 encoded Ca²⁺ indicators. *J Neurosci* **24**, 9572-9579 (2004).
- 278 6. Tian L, Akerboom J, Schreier ER, Looger LL. Neural activity imaging with genetically encoded
279 calcium indicators. *Prog Brain Res* **196**, 79-94 (2012).
- 280 7. Deo C, Lavis LD. Synthetic and genetically encoded fluorescent neural activity indicators. *Curr*
281 *Opin Neurobiol* **50**, 101-108 (2018).
- 282 8. Broussard GJ, Liang R, Tian L. Monitoring activity in neural circuits with genetically encoded
283 indicators. *Front Mol Neuro* **7**, 1-17 (2014).
- 284 9. Kim TH, *et al.* Long-Term Optical Access to an Estimated One Million Neurons in the Live Mouse
285 Cortex. *Cell Rep* **17**, 3385-3394 (2016).
- 286 10. Podor B, Hu YL, Ohkura M, Nakai J, Croll R, Fine A. Comparison of genetically encoded calcium
287 indicators for monitoring action potentials in mammalian brain by two-photon excitation
288 fluorescence microscopy. *Neurophotonics* **2**, 1-7 (2015).
- 289 11. Bootman MD, Allman S, Rietdorf K, Bultynck G. Deleterious effects of calcium indicators within
290 cells; an inconvenient truth. *Cell Calcium* **73**, 82-87 (2018).
- 291 12. Steinmetz NA, *et al.* Aberrant Cortical Activity in Multiple GCaMP6-Expressing Transgenic Mouse
292 Lines. *eNeuro* **4**, 1-15 (2017).
- 293 13. Helmchen F, Imoto K, Sakmann B. Ca²⁺ buffering and action potential-evoked Ca²⁺ signaling in
294 dendrites of pyramidal neurons. *Biophys J* **70**, 1069-1081 (1996).
- 295 14. Ashworth R, Zimprich F, Bolsover SR. Buffering intracellular calcium disrupts motoneuron
296 development in intact zebrafish embryos. *Dev Brain Res* **129**, 169-179 (2001).
- 297 15. Briston SJ, Dibb KM, Solaro RJ, Eisner DA, Trafford AW. Balanced changes in Ca buffering by
298 SERCA and troponin contribute to Ca handling during β -adrenergic stimulation in cardiac
299 myocytes. *Cardiovascular Res* **104**, 347-354 (2014).
- 300 16. Timofeeva Y, Volynski KE. Calmodulin as a major calcium buffer shaping vesicular release and
301 short-term synaptic plasticity: facilitation through buffer dislocation. *Front Cell Neuro* **9**, 239-239
302 (2015).
- 303 17. Yang Y, *et al.* Improved calcium sensor GCaMP-X overcomes the calcium channel perturbations
304 induced by the calmodulin in GCaMP. *Nat Commun* **9**, 1-18 (2018).
- 305 18. Barykina NV, *et al.* A new design for a green calcium indicator with a smaller size and a reduced
306 number of calcium-binding sites. *Sci Rep* **6**, 1-15 (2016).
- 307 19. Barykina NV, *et al.* NTnC-like genetically encoded calcium indicator with a positive and enhanced
308 response and fast kinetics. *Sci Rep* **8**, 1-19 (2018).
- 309 20. Dana H, *et al.* High-performance calcium sensors for imaging activity in neuronal populations
310 and microcompartments. *Nat Methods* **16**, 649-657 (2019).
- 311 21. Shaner NC, *et al.* A bright monomeric green fluorescent protein derived from *Branchiostoma*
312 *lanceolatum*. *Nat Methods* **10**, 407-409 (2013).
- 313 22. Wu J, *et al.* A long Stokes shift red fluorescent Ca²⁺ indicator protein for two-photon and
314 ratiometric imaging. *Nat Commun* **5**, 1-11 (2014).
- 315 23. Clavel D, *et al.* Structural analysis of the bright monomeric yellow-green fluorescent protein
316 mNeonGreen obtained by directed evolution. *Acta Crystallogr, Sect D* **72**, 1298-1307 (2016).
- 317 24. Ai H-w, Baird MA, Shen Y, Davidson MW, Campbell RE. Engineering and characterizing
318 monomeric fluorescent proteins for live-cell imaging applications. *Nat Protoc* **9**, 910-928 (2014).

- 319 25. Palmer AE, Tsien RY. Measuring calcium signaling using genetically targetable fluorescent
320 indicators. *Nat Protoc* **1**, 1057-1065 (2006).
- 321 26. Kawakami K, Takeda H, Kawakami N, Kobayashi M, Matsuda N, Mishina M. A Transposon-
322 Mediated Gene Trap Approach Identifies Developmentally Regulated Genes in Zebrafish. *Dev*
323 *Cell* **7**, 133-144 (2004).
- 324 27. Pachitariu M, *et al.* Suite2p: beyond 10,000 neurons with standard two-photon microscopy.
325 *bioRxiv*, 1-30 (2017).
- 326 28. Shinnawi R, *et al.* Monitoring Human-Induced Pluripotent Stem Cell-Derived Cardiomyocytes
327 with Genetically Encoded Calcium and Voltage Fluorescent Reporters. *Stem Cell Reports* **5**, 582-
328 596 (2015).
- 329 29. Chang Y-F, *et al.* Non-invasive phenotyping and drug testing in single cardiomyocytes or beta-
330 cells by calcium imaging and optogenetics. *PLOS ONE* **12**, 1-17 (2017).
- 331 30. Smith NA, Kress BT, Lu Y, Chandler-Militello D, Benraiss A, Nedergaard M. Fluorescent Ca²⁺
332 indicators directly inhibit the Na,K-ATPase and disrupt cellular functions. *Science Signaling* **11**, 1-
333 14 (2018).
- 334 31. Cranfill PJ, *et al.* Quantitative assessment of fluorescent proteins. *Nat Methods* **13**, 557-562
335 (2016).
- 336 32. Tsien R, Pozzan T. [14] Measurement of cytosolic free Ca²⁺ with quin2. In: *Methods Enzymol.*
337 Academic Press (1989).
- 338 33. Dweck D, Reyes-Alfonso A, Potter JD. Expanding the range of free calcium regulation in
339 biological solutions. *Anal Biochem* **347**, 303-315 (2005).
- 340 34. Xu C, Webb WW. Measurement of two-photon excitation cross sections of molecular
341 fluorophores with data from 690 to 1050 nm. *J Opt Soc Am B: Opt Phys* **13**, 481-491 (1996).
- 342 35. Mütze J, *et al.* Excitation Spectra and Brightness Optimization of Two-Photon Excited Probes.
343 *Biophysical Journal* **102**, 934-944 (2012).
- 344 36. Palmer AE, Tsien RY. Measuring calcium signaling using genetically targetable fluorescent
345 indicators. *Nat Protoc* **1**, 1057-1065 (2006).
- 346 37. Wardill TJ, *et al.* A Neuron-Based Screening Platform for Optimizing Genetically-Encoded
347 Calcium Indicators. *PLOS ONE* **8**, e77728 (2013).
- 348 38. Thorn RJ, Clift DE, Ojo O, Colwill RM, Creton R. The loss and recovery of vertebrate vision
349 examined in microplates. *PLOS ONE* **12**, 1-17 (2017).

351 **Methods**

352 **General procedures**

353 Synthetic DNA oligonucleotides and gBlocks were purchased from Integrated DNA
354 Technologies. Plastic consumables, restriction endonucleases, Taq polymerase, Phusion
355 polymerase, T4 DNA ligase, deoxynucleotides, DH10B *E. coli*, pBAD/His B plasmid,
356 pcDNA3.1(+) plasmid, Bacterial Protein Extraction Reagent (B-PER), Penicillin-Streptomycin,
357 Fetal Bovine Serum (FBS), TurboFect, Lipofectamine 2000, and GeneJet gel or plasmid
358 purification kits were purchased from Thermo Scientific. Endotoxin-free plasmid DNA isolation
359 kits were purchased from Qiagen (cat. 12362). Agarose, $MnCl_2 \cdot 4H_2O$, tryptone, D-glucose,
360 ampicillin, L-arabinose, Hank's balanced salt solution (HBSS), DMEM, TrypLE Express, and LB
361 Lennox media were purchased from Fisher Scientific. NbActiv4 and neuron transfection media
362 were purchased from Brain Bits.

363 3-(N-morpholino)propanesulfonic acid (MOPS), ethylene glycol-bis(2-aminoethylether)-
364 N,N,N',N'-tetraacetic acid (EGTA), and nitrilotriacetic acid (NTA), were purchased from VWR.
365 Nickel NTA immobilized metal affinity chromatography protein purification beads were
366 purchased from G-BioSciences. Ionomycin and tricaine methanesulfonate were purchased from
367 Millipore-Sigma. Ethidium bromide and PCR machines (T100 Thermal Cycler) were purchased
368 from BioRad. Gibson Assembly reagent was purchased from New England Biolabs (NEB).
369 Genemorph II Random Mutagenesis kits and QuikChange mutagenesis kits were purchased
370 from Agilent Technologies. Nunc 96-Well Polypropylene DeepWell Storage Plates (cat. 278743)
371 and 96-well Nunc MicroWell 96-Well Optical-Bottom Plates (cat. 265301) were purchased from
372 Thermo Scientific. Molecular weight cut off filters were purchased from Millipore-Sigma.
373 Sequencing was completed by the Molecular Biology Services Unit at the University of Alberta.

374 **Molecular biology and protein engineering**

375 Libraries for iterative directed evolution were created using Genemorph II Random Mutagenesis
376 kits and NEB's Gibson Assembly reagent. Blunt ended linear DNA fragments with random
377 mutations are created using the Genemorph II kit according to the manufacturer's
378 recommendations. Genemorph II PCR product was ligated using NEB Gibson Assembly
379 reagent into a linearized pBAD vector cut with XhoI/HindIII. Site saturation mutagenesis libraries
380 were created using single and multi QuikChange mutagenesis kits according the manufacturers
381 recommendations.

382 Libraries are transformed into DH10B *E. coli* and plated on 100 µg/L ampicillin/1.5% agar plates
383 with 0.02% L-arabinose and grown overnight (12-18 hours) at 37 °C. Colonies are selected on
384 the basis of fluorescence intensity, picked, and placed into 96 DeepWell blocks containing 1.3
385 mL of LB Lennox media supplemented with 100 µg/mL ampicillin and 0.02% L-arabinose.
386 Deepwell blocks were shaken overnight at 37 °C. The next day, blocks are centrifuged at 6000
387 × g for 5 minutes to pellet cells. Media was discarded and 30 µL of B-PER was added to each
388 well. After shaking for 15 minutes, 200 µL of 10 mM EGTA in 30 mM MOPS/100 mM KCl pH 7.2
389 (MOPS/KCl buffer) is added to each well of the blocks before mixing briefly and being
390 centrifuged again for 5 minutes at 6000 × g. 90 µL of the resulting lysate is loaded in each well
391 of 96-well optical bottom plates. Fluorescence intensity for each well of the plate is then read
392 with a Tecan Safire² microplate reader to determine the low Ca²⁺ intensity for each variant. High
393 Ca²⁺ intensity is acquired by adding 15 µL of 100 mM Ca²⁺ in 30 mM MOPS pH 7.2 with a 60
394 second shake before reading. Taking the value of the high Ca²⁺ intensity divided by the low Ca²⁺
395 intensity gives a relative sensitivity value. Promising candidates, usually 10% of each 96-well
396 block, are retested from the lysate in 10 mM low (EGTA chelated) and 10 mM high Ca²⁺ solution
397 diluted in MOPS/KCl buffer. The plasmids associated with the promising variants are sent for
398 sequencing and used as template for the next round of directed evolution. For cultured neuron
399 field stimulation experiments, GCaMP6s, jGCaMP7f, jGCaMP7s, jGCaMP7c, and jGCaMP7b
400 plasmids (available on Addgene) were subcloned into a syn-<GCaMP>-IRES-mCherry-WPRE-
401 pA vector.

402 Constructs for zebrafish transfection were created by ligating mNG-GECO1 PCR product into a
403 Tol2 transposon backbone. Briefly, PCR of mNG-GECO variants were ligated into Tol2-HuC-
404 H2B vector (Addgene plasmid #59530) cut with Sall/Agel using Gibson Assembly. The ligated
405 constructs were transformed into NEB Turbo Competent *E. coli* cells and grown in 250 µL
406 culture overnight at 30 °C. The next day, the culture is pelleted, and the DNA is purified using
407 endotoxin-free plasmid DNA purification protocol using EndoFree Plasmid Maxi Kit. The DNA is
408 eluted with EF-free H₂O and verified by sequencing.

409 **Protein purification and *in vitro* characterization**

410 To purify mNG, mNG-GECO variants, and GCaMP6s for *in vitro* characterization, pBAD/His B
411 plasmid containing the gene of interest was used to transform electrocompetent DH10B *E. coli*,
412 which were then streaked on 100 µg/mL ampicillin/1.5% agar plates. After overnight incubation
413 at 37 °C, a single colony was picked and inoculated to a 2 L flask containing 500 mL of 100

414 $\mu\text{g/mL}$ ampicillin/0.02% L-arabinose liquid media and cultured for 24-30 hours at 37 °C. The
415 culture is then centrifuged at $6000 \times g$ for 6 minutes to collect the cells. Cells are re-suspended
416 in 30 mL of cold Tris buffered saline (TBS, 150 mM NaCl, 50 mM Tris-HCl) pH 8.0 and lysed by
417 sonication (QSonica Q700, amplitude 50, 1 second on, 2 seconds off, 3 minutes sonication
418 time). All subsequent purification procedures were performed on ice. The resulting lysate was
419 clarified of cell debris by centrifugation for 1 hour at $21,000 \times g$, filtered through a Kim-wipe into
420 a 50 mL conical bottom tube, and incubated for 3 hours with Ni-NTA resin. Resin containing
421 NTA bound protein was washed with 100 mL of 20 mM imidazole TBS wash buffer and eluted
422 with 250 mM imidazole TBS elution buffer. Purified protein was buffer exchanged into TBS
423 using a 10,000 Da molecular weight cut-off filter (Millipore-Sigma) through 3 successive
424 washes. Absorption spectra were recorded on a Beckman-Coulter DU-800 UV-visible
425 spectrophotometer and fluorescence spectra recorded on a Tecan Safire² plate reader.

426 Extinction coefficient determination for mNG-GECO variants were performed using the alkaline
427 denaturation method with mNG as a standard³¹. Briefly, the concentration of protein was
428 adjusted by dilution in MOPS/KCl pH 7.2 to reach an absorbance of 0.6 to 1.0. A dilution series
429 with MOPS/KCl and 10 mM Ca^{2+} was then prepared with absorbances of 0.01, 0.02, 0.03, 0.04,
430 and 0.05 for mNG, mNG-GECO variants, and GCaMP6s. Integration of the fluorescent peaks
431 provides a total fluorescent emission value which was plotted against the absorbance to provide
432 a slope. The quantum yields of mNG-GECO variants were determined using the published³¹ QY
433 value of mNG in a ratiometric manner:

434
$$\Phi_{\text{protein}} = \Phi_{\text{standard}} \times (S_{\text{protein}}/S_{\text{standard}})$$

435 Extinction coefficients were determined by measuring the absorption spectrum in MOPS/KCl pH
436 7.2 and 2 M NaOH. The absorbance value for the denatured GFP peak at 440 nm was divided
437 by the previously determined extinction coefficient of $44,000 \text{ M}^{-1}\text{cm}^{-1}$ to give the concentration of
438 protein³¹. Using Beer's law, the extinction coefficient was then determined by dividing the TBS
439 sample absorbance maximum by the calculated protein concentration.

440 Determination of K_d was performed as previously described^{32, 33}. Briefly, a reciprocal dilution
441 series was created with either 10 mM EGTA/10 mM Ca^{2+} EGTA ranging in free Ca^{2+}
442 concentration of 0 to 0.039 mM or 10 mM NTA/10 mM Ca^{2+} NTA ranging in free Ca^{2+}
443 concentration from 0 to 1.13 mM³³. An equal amount of purified mNG-GECO was diluted 100×

444 into 100 μL of buffer and the intensity plotted against free Ca^{2+} in triplicate. The data are then fit
445 to a four-parameter variable-slope in GraphPad Prism 7 software to determine the K_d .

446 **Two Photon Measurements**

447 The two photon measurements were performed in 39 μM free Ca^{2+} (+ Ca^{2+}) buffer (30 mM
448 MOPS, 10 mM CaEGTA in 100 mM KCl, pH 7.2) or 0 μM free Ca^{2+} (- Ca^{2+}) buffer (30 mM
449 MOPS, 10 mM EGTA in 100 mM KCl, pH 7.2). The two photon excitation spectra were acquired
450 as previously described². Protein solution of 2 – 4 μM concentration in + Ca^{2+} or - Ca^{2+} buffer was
451 prepared and measured using an inverted microscope (IX81, Olympus) equipped with a 60 \times ,
452 1.2 NA water immersion objective (Olympus). Two photon excitation was obtained using an 80
453 MHz Ti-Sapphire laser (Chameleon Ultra II, Coherent) for spectra from 710 nm to 1080 nm.
454 Fluorescence collected by the objective was passed through a short pass filter (720SP,
455 Semrock) and a band pass filter (550BP200, Semrock), and detected by a fiber-coupled
456 Avalanche Photodiode (APD) (SPCM_AQRH-14, Perkin Elmer). The obtained two photon
457 excitation spectra were normalized for 1 μM concentration and further used to obtain the action
458 cross-section spectra (AXS) with fluorescein as a reference³⁴.

459 Fluorescence correlation spectroscopy (FCS) was used to obtain the 2P molecular brightness of
460 the protein molecule. The molecular brightness was defined by the rate of fluorescence
461 obtained per total number of emitting molecules. 50-200 nM protein solutions were prepared in
462 + Ca^{2+} buffer and excited with 940 nm wavelength at various power ranging from 2-30 mW for
463 200 seconds. The obtained fluorescence was collected by an APD and fed to an autocorrelator
464 (Flex03LQ, Correlator.com). The obtained autocorrelation curve was fit on a diffusion model
465 through an inbuilt Matlab function³⁵ to determine the number of molecules $\langle N \rangle$ present in the
466 focal volume. The 2-photon molecular brightness (ϵ) at each laser power was calculated as the
467 average rate of fluorescence $\langle F \rangle$ per emitting molecule $\langle N \rangle$, defined as $\epsilon = \langle F \rangle / \langle N \rangle$ in
468 kilocounts per second per molecule (kcpsm). As a function of laser power, the molecular
469 brightness initially increases with increasing laser power, then levels off and decreases due to
470 photobleaching or saturation of the protein chromophore in the excitation volume. The maximum
471 or peak brightness achieved, $\langle \epsilon_{max} \rangle$, represents a proxy for the photostability of a fluorophore.

472 ***In vitro* kinetics analysis by stopped-flow**

473 Rapid kinetic measurements of purified mNG-GECO1 and GCaMP6s were made using an
474 Applied Photophysics SX-20 Stopped-flow Reaction Analyzer exciting at 488 nm with 2 nm

475 bandwidth and collecting light at 520 nm through a 10 mm path at room temperature. Briefly, 2
476 μM of mNG-GECO1 and GCaMP6s proteins in 1 mM Ca^{2+} (30 mM MOPS, 100 mM KCl, pH 7.2)
477 were rapidly mixed at 1:1 ratio with 50 mM of EGTA (same buffer as above) at room
478 temperature. k_{off} values were determined by fitting a single exponential dissociation curve to the
479 signal decay using Graphpad Prism, with units of s^{-1} . For k_{on} , both proteins buffered in 30 mM
480 MOPS, 100 mM KCl, 50 μM EGTA were rapidly mixed at 1:1 ratio with varying concentrations of
481 Ca^{2+} produced by reciprocal dilutions of 10 mM EGTA and 10 mM CaEGTA. The measured
482 fluorescence change overtime was fitted using a 2-phase association curve to obtain the slow
483 and fast observed rate constants (k_{obs}) for each free Ca^{2+} concentration. All measurements were
484 done in triplicates, and values are reported as mean \pm s.e.m. where noted.

485 **Fluorescence live cell imaging**

486 **Imaging in HeLa cells.** We followed previously reported protocols for our Ca^{2+} imaging
487 experiments³⁶. Briefly, HeLa cells cultured in DMEM with 10% fetal bovine serum supplemented
488 with penicillin-G potassium salt (50 units/mL) and streptomycin sulphate (50 $\mu\text{g}/\text{mL}$) were plated
489 on collagen coated 35 mm glass bottom dishes. HeLa cells are transfected at 60% confluency
490 with 1 μg of pcDNA3.1(+) harboring the variant of interest using 2 μL of TurboFect according to
491 the manufacturer's recommendation. After overnight incubation at 37 °C with 5% CO_2 , cells
492 were washed twice with prewarmed Hank's balanced salt solution immediately before imaging.

493 Imaging of transfected HeLa cells was performed on an inverted Zeiss 200M microscope with
494 Semrock filters (excitation 470/40, emission 525/50) and captured with an OrcaFlash 4.0 –
495 C13440 (Hamamatsu). Images were acquired through a 40 \times (N.A. 1.3) oil immersion lens using
496 MetaMorph 7.8.0.0 software and an MS-2000 automated stage (Applied Scientific
497 Instrumentation).

498 **Imaging in dissociated rat cortical neurons.**

499 The mNG-GECO1 indicator was compared to other GECIs in a field stimulation assay³⁷.
500 Neonatal (P0) rat pups were euthanized, and their cortices were dissected and dissociated
501 using papain (Worthington). Cells were transfected by combining 5×10^5 viable cells with 400 ng
502 plasmid DNA and nucleofection solution electroporation cuvettes (Lonza). Electroporation was
503 performed according to the manufacturer instructions. Cells were then plated at a density of
504 5×10^5 cells/well in poly-D-lysine (PDL) coated 96-well plates. After 14-18 days in vitro, culture
505 medium was exchanged for an imaging buffer solution with a drug cocktail to inhibit synaptic

506 transmission³⁷. The field stimulation assay was performed as previously described^{4, 20, 37}. Briefly,
507 neurons were field stimulated (1, 2, 3, 5, 10, 20, 40, 160 pulses at 83 Hz, 1 ms, 40V), and
508 concurrently imaged with an electron multiplying charge coupled device (EMCCD) camera
509 (Andor iXon DU897-BV, 198 Hz, 4x4 binning, 800 x 800 μm , 1,400 frames). Reference images
510 were taken after stimulation to perform cell segmentation during analysis. Illumination was
511 delivered by blue light (470 nm, Cairn Research Ltd; excitation: 450-490 nm; emission: 500-550
512 nm; dichroic: 495 nm long-pass). The illumination power density was measured to be 19
513 mW/mm^2 at the sample. Stimulation pulses were synchronized with the camera using data
514 acquisition cards (National Instruments), controlled with Wavesurfer software
515 (<https://wavesurfer.janelia.org/>). Imaging was performed at room temperature. Data were
516 analyzed using previously-developed MATLAB (Mathworks) scripts^{20, 37}.

517 **Ca²⁺ imaging in human iPSC-derived cardiomyocytes**

518 Human iPSC-derived cardiomyocytes (human iPSC Cardiomyocytes - male | ax2505) were
519 purchased from Axol Bioscience. The 96 well glass-bottom plate or MatTek glass bottom dish
520 (Ashland, MA, US) were first coated with Fibronectin/Gelatin (0.5% / 0.1%) at 37 °C for at least
521 1 hour. The cells were plated and cultured for three days in Axol's Cardiomyocyte Maintenance
522 Medium. The cells then were ready for final observation with Tyrode's buffer. For electrical
523 stimulations, iPSC derived cardiomyocytes were plated on MatTek glass bottom dish (Ashland,
524 MA, US) at 100,000 cells/well. Electrical stimulation was done with 10 V, 10 ms duration and 3
525 seconds interval using myopacer (Ion optix c-pace ep). To image, an inverted microscope
526 (DMI8, Leica) equipped with a 63x objective lens (NA 1.4) and a multiwavelength LED light
527 source (pE-4000, CoolLED) was used. iPSC derived cardiomyocytes were plated out as above,
528 and then loaded with 5 μM Fluo-4-AM (Thermo-Fisher, UK) at room temperature for 10 minutes,
529 free dye was washed off by media replacement with pre-heated culture media, followed by
530 imaging with iXon EMCCD (Andor) camera using 488 nm LED illumination. The GFP filter set
531 (DS/FF02-485/20-25, T495lpxr dichroic mirror, and ET525/50 emission filter) was used for Fluo-
532 4 and mNG-GECO1 observation.

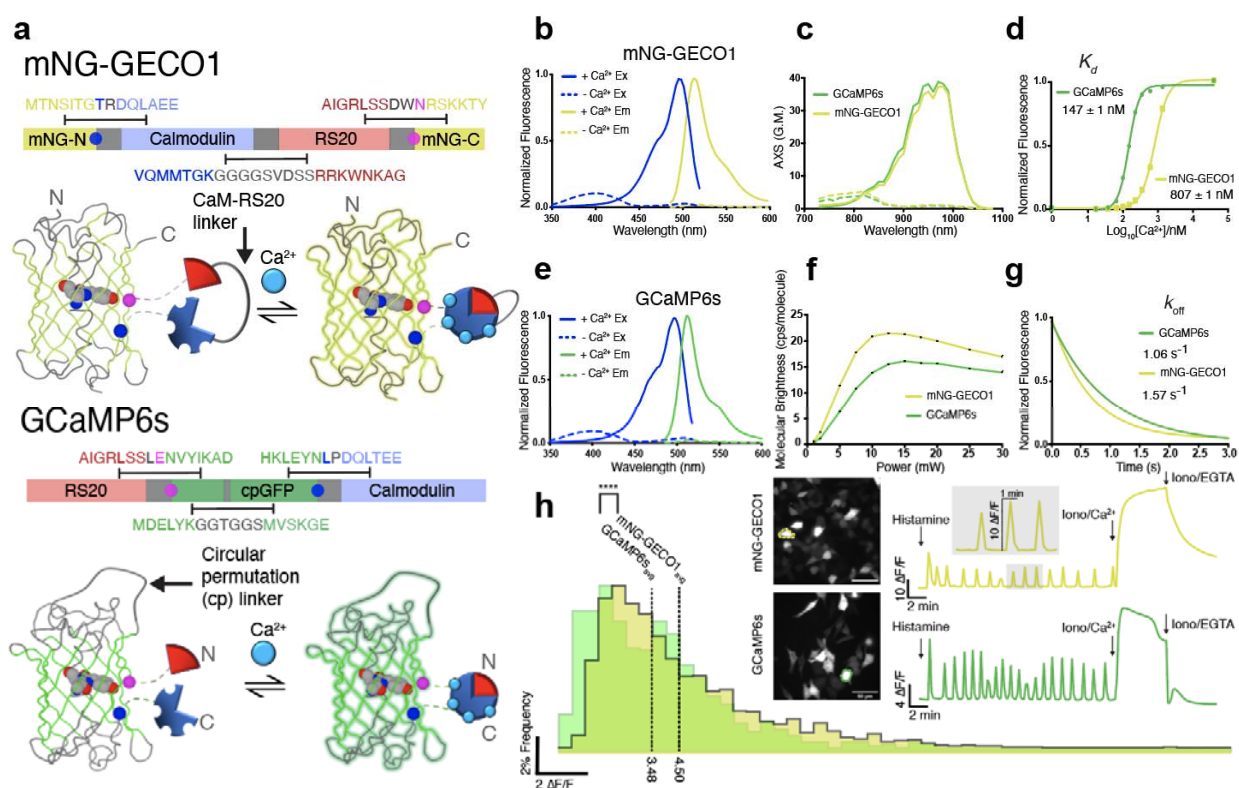
533 **Imaging of zebrafish larvae.**

534 To demonstrate the sensitivity and brightness of mNG-GECO1 *in vivo*, we performed
535 fluorescence imaging of Ca²⁺ activity in a subset of neurons in larval zebrafish. Initially, we used
536 the AB/WIK zebrafish strain for morphology studies (**Supplementary Fig. 4**), which were
537 treated with 1-phenol-2-thiourea (PTU) to inhibit pigmentation, as described previously³⁸. Later,

538 *Casper* strains were available and 20 ng/μL DNA plasmids encoding mNG-GECO1 under the
539 control of nuclear-localized *elavl3*/HuC promoter (Addgene: 59530) were injected into two-cell
540 stage embryos of *Casper* mutant zebrafish³³ with 40 ng/μl Tol2 transposase mRNA (26) to
541 generate F0 transgenic zebrafish. Imaging experiments were performed using 6 day old
542 embryos. Embryos showing expression were treated with 1 mg/mL bath-applied α-bungarotoxin
543 (Thermo Fischer Scientific, B1601) dissolved in external solution for 30 seconds to block
544 movement, and subsequently incubated with 80 mM 4-aminopyridine (4AP) for 10 minutes.
545 After incubation, the larvae were embedded in 2% low melting temperature agarose to prevent
546 motion. For earlier imaging (**Supplementary Fig. 4**) a Zeiss 700 confocal microscope was used
547 with A-Plan 10x/0.25 Ph1 M27 objective lens to obtain picture from the whole larvae
548 (**Supplementary Fig. 4a**). For enlarged areas (**Supplementary Fig. 4b-e**), a Plan-Apochromat
549 20x/0.8 M27 lens was used. Later imaging was performed using a 488 nm laser (0.45 μM) and a
550 525/50 nm emission filter at 3 Hz using Zeiss 880 confocal microscope. The laser power was
551 set to 2.3%, gain 720, and pinhole to 29.3% open. Image acquisition, data registration,
552 segmentation and cell traces were handled using theSuite2p package in Python. All animal
553 procedures were approved by the Institutional Animal Care and Use Committee at the HHMI
554 Janelia Research Campus or by the Animal Care and Use Committee: Biosciences at the
555 University of Alberta.

556 **Figures and Supplementary Data**

557

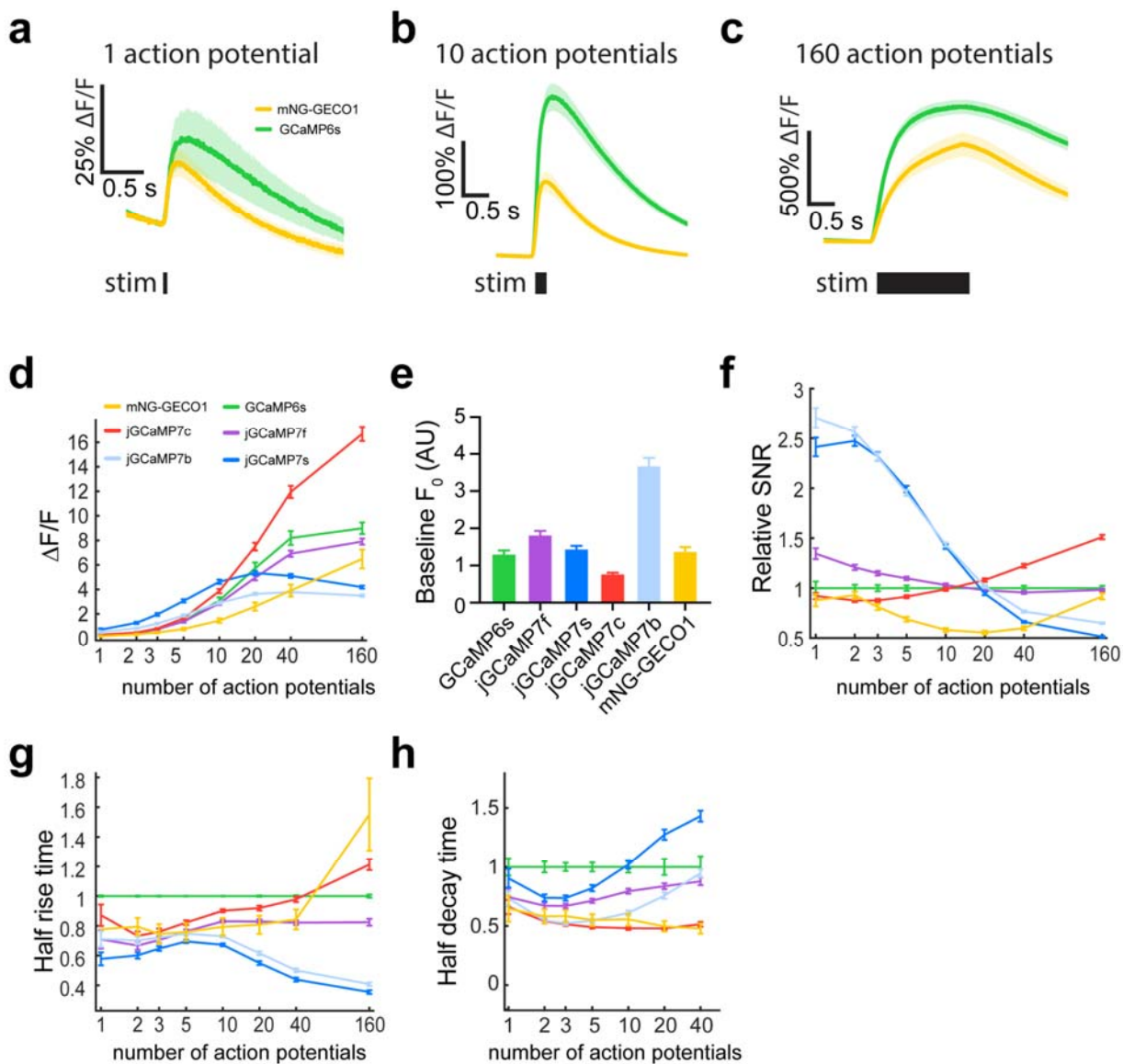


558

559 **Figure 1 Topology and *in vitro* characterization of mNG-GECO1 and GCaMP6s**

560 **a** Topology of non-circularly permuted mNG-GECO1 and circularly permuted GCaMP6s. Linker
 561 regions are shown in grey and the two residues that flank the insertion site (residue 136 of mNG
 562 in blue and residue 139 in magenta; numbering as in PDB ID 5LTR)²³ are shown as circles on
 563 both the protein structure and gene schematics. The Ca²⁺ responsive domains are shaded light
 564 blue for CaM and light red for RS20. **b,e** Excitation and emission spectra for each indicator. **c** 2-
 565 photon cross section for each indicator in Ca²⁺ saturated or Ca²⁺ free states. **d** Ca²⁺ titration for
 566 GCaMP6s ($K_d = 147 \pm 1$ nM) and mNG-GECO1 (807 ± 1 nM). **f** Dependence of two-photon
 567 molecular brightness on excitation power intervals. **g** Stop-flow kinetics for each indicator
 568 showing mNG-GECO1 ($k_{off} 1.57$ s⁻¹) and GCaMP6s ($k_{off} 1.06$ s⁻¹). **h** Characterization of
 569 histamine induced Ca²⁺ oscillations in HeLa cells with representative traces inset.

570



571

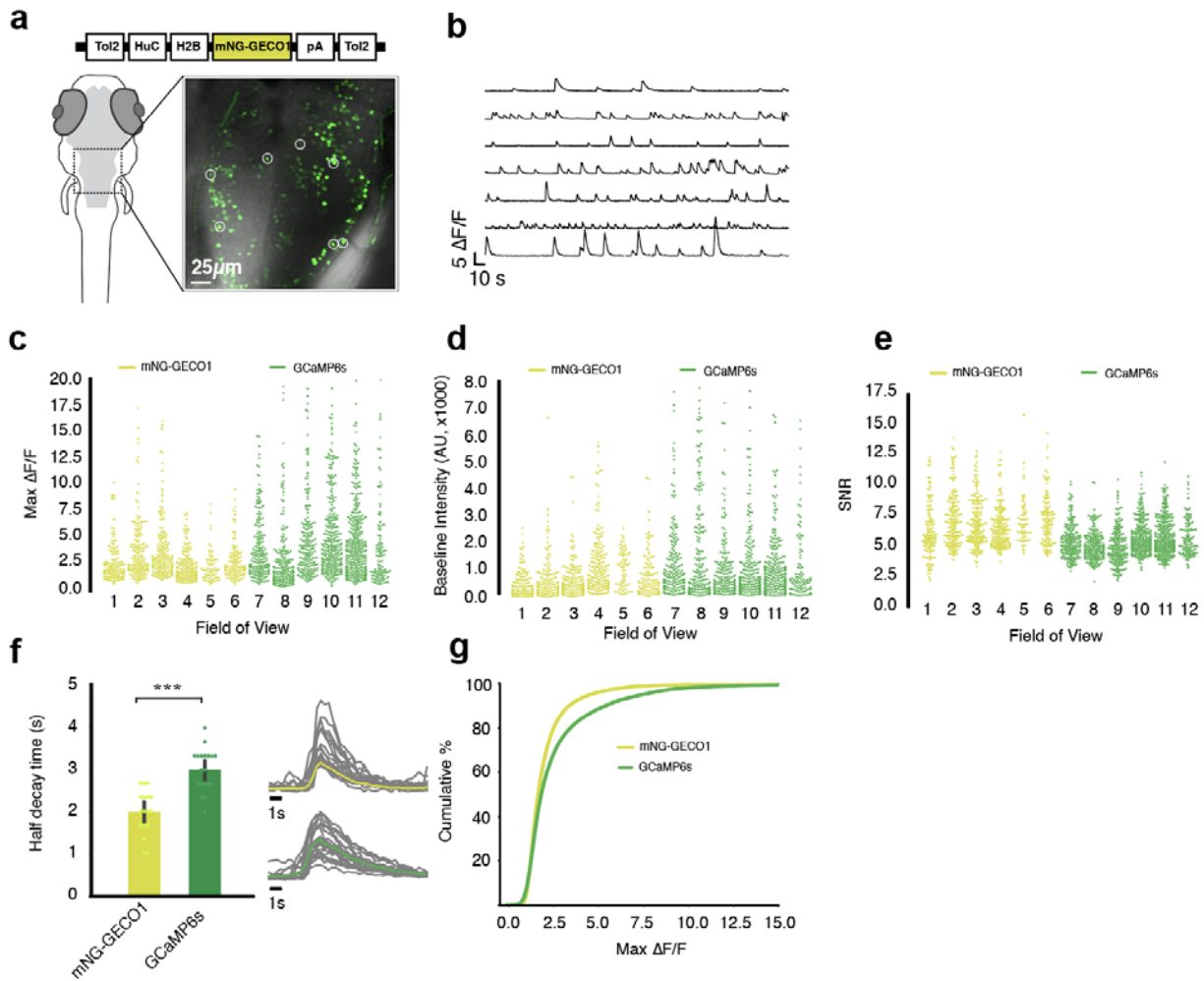
572 **Figure 2 Characterization of mNG-GECO1 and GCaMP series indicators in dissociated rat**
573 **hippocampal neurons**

574 **a-c** Average responses to 1, 10, and 160 action potentials for mNG-GECO1 and GCaMP6s.
575 Shaded areas correspond to s.e.m. for each trace. **d** Response amplitude $\Delta F/F_0$ for mNG-
576 GECO1 and the GCaMP series of indicators in response to 1, 2, 3, 5, 10, 20, 40, and 160 action
577 potentials. Data are presented normalized to $\Delta F/F_0$ of GCaMP6s. **e** Baseline brightness for each
578 indicator, defined as the mean raw fluorescence intensity of all neurons prior to the stimulus. **f**
579 Relative SNR, defined as the peak raw fluorescence divided by the signal standard deviation
580 prior to the stimulus, normalized to SNR of GCaMP6s. **g** Half-rise time normalized to GCaMP6s.

581 **h** Half-decay time normalized to GCaMP6s. The 160 action potential measurement was omitted
582 because fluorescence levels generally did not return to baseline over the imaging period. For **a-**
583 **h**, mNG-GECO1: 621 neurons, 15 wells; GCaMP6s: 937 neurons, 17 wells; jGCaMP7c: 2,551
584 neurons, 44 wells; jGCaMP7b: 2,339 neurons, 47 wells; jGCaMP7f: 2,585 neurons, 48 wells;
585 and jGCaMP7s: 2,249 neurons, 47 wells. Data in **d-h** shown as mean \pm s.e.m., see
586 **Supplementary Table 3** for analyzed data.

587

588



589

590 **Figure 3 Characterization of mNG-GECO1 and GCaMP6s in transgenic zebrafish hind**
 591 **brain tissue.** **a** Schematic representation of Tol2[HuC-H2B-mNG-GECO1] construct and
 592 confocal image of one fish (5 to 6 days post fertilization) with 7 region of interests (ROI) circled.
 593 **b** Traces of ROI's from a). **c** Max $\Delta F/F_0$ calculated by taking the max peak of each cell within the
 594 field of interest over 5 minutes; six ROI's each are used from 5 independent fish expressing
 595 mNG-GECO1 and 5 fish expressing GCaMP6s. **d** Baseline fluorescence intensity of each cell
 596 within all ROI's from 5 fish; confocal settings are kept consistent between GCaMP6s and mNG-
 597 GECO1 imaging. **e** Signal-to-noise ratio (SNR) computed by dividing $\Delta F/F_0$ by raw standard
 598 deviation of each cell across 6 FOV's each for both sensors. **f** Average half decay time plotted
 599 for mNG-GECO1 ($n = 17$) and GCaMP6s ($n = 19$) by averaging randomly selected peaks. **g**

600 Cumulative distribution of mNG-GECO1 vs. GCaMP6s. All cells are arranged in incremental
601 order of $\Delta F/F_0$ and plotted with respect to their $\Delta F/F_0$ and their position in the order (%).

602 **Supplementary Figures and Tables**

603 **Supplementary Table 1. In vitro characterization of mNG-GECO1 and GCaMP6s.** mNG,
 604 mNG-GECO1, and GCaMP6s were purified and tested in parallel. mNG was used as a standard
 605 for brightness and quantum yield determination.

Indicator	Excitation Maximum (nm) (C/a ²)		Emission Maximum (nm) (C/a ²)	Quantum Yield (Ca ²⁺ sat.)	Fluorescence		Brightness Relative to GCaMP6s	Brightness Relative to mNG	K _d (nM)	k _{off} (s ⁻¹)
	λ _{exc}	λ _{exc}			ε (mM ⁻¹ cm ⁻¹); Ca ²⁺ sat.)	Brig htness ^a				
mNeonGreen	506	517	0.8 ^b	112,000 +/- 900	90	205%	100%	NA	NA	NA
mNG-GECO1	496	513	0.69 +/- 0.01	102,000 +/- 2,700	70	159%	78%	35	807 +/- 1	1.57 +/- 0.01
GCaMP6s	497	512	0.59 +/- 0.02	74,000 +/- 500	44	100%	49%	39	147 +/- 1	1.06 +/- 0.01

^aProduct of ε in mM⁻¹cm⁻¹ and Φ (no units)

^bFrom Ref.²¹

606

607 **Supplementary Table 2. Characterization of Ca²⁺-dependent fluorescence of mNG-GECO1**
608 **and GCaMP6s in HeLa cells.** Cells were treated with histamine (abb. His), then with
609 Ca²⁺/ionomycin (abb. Ca²⁺), and then with EGTA/ionomycin (abb. EGTA). n is the total number
610 of cells recorded over five independent transfections. The oscillations were detected in all cells
611 with a prominence of greater than 0.5 using a Matlab script. Errors are s.d.

Protein	Number of HeLa cells (n)	Total Number of oscillations detected	Maximum Ca ²⁺ to minimum EGTA $\Delta F/F_0$	Maximum His to minimum His ratio	Maximum His to maximum Ca ²⁺ ratio
mNG-GECO1	137	1624	4.50 ± 2.96	48.8 ± 15.1	16.8 ± 10.5
GCaMP6s	99	687	3.48 ± 2.40	16.7 ± 5.2	12.8 ± 6.11

612

613 **Supplementary Table 3. mNG-GECO1 comparison with GCaMP series sensors in**
 614 **dissociated rat hippocampal neurons.** Median values were calculated per well and mean (of
 615 medians) \pm s.e.m. are presented. SNR values were calculated per individual cells, and median \pm
 616 s.e.m are shown.

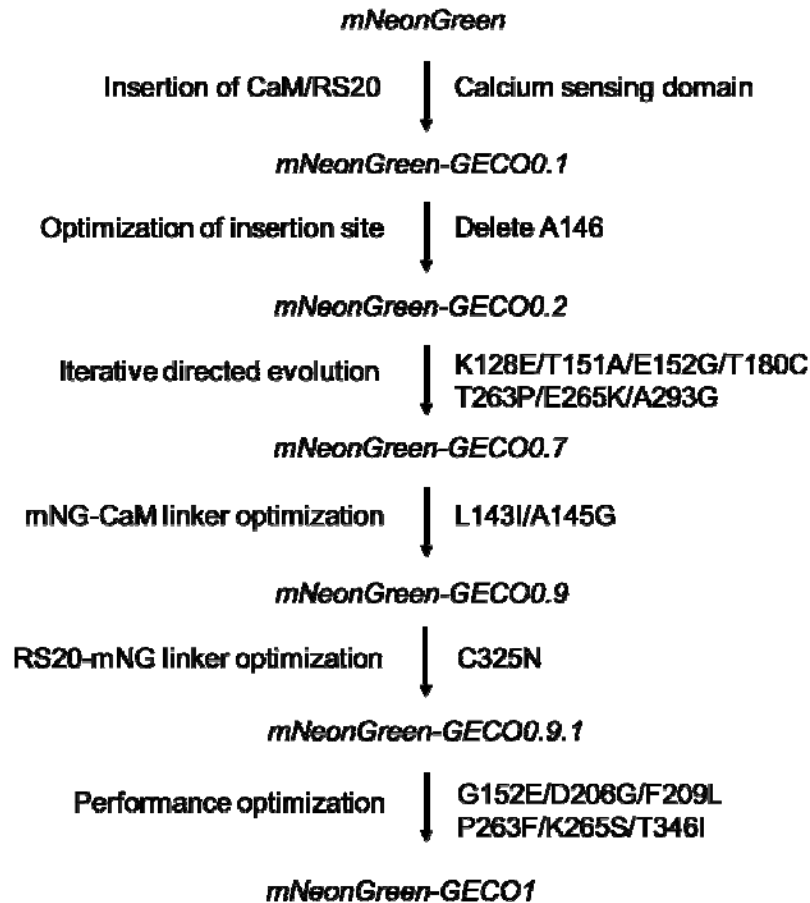
Protein	1 AP $\Delta F/F_0$ amplitude	3 AP $\Delta F/F_0$ amplitude	10 AP $\Delta F/F_0$ amplitude	160 AP $\Delta F/F_0$ amplitude	Baseline Brightness (Fluorescence Intensity (AU))	Half rise time 3 APs (ms)	Half decay time 3 APs (ms)	SNR 1 APs	SNR 3 APs
mNG- GECO1	0.19 \pm 0.04	0.5 \pm 0.07	1.5 \pm 0.19	6.5 \pm 0.8	1374 \pm 31	49 \pm 1	582 \pm 12	8.9 \pm 0.01	20.3 \pm 0.02
GCaMP6s	0.27 \pm 0.09	0.7 \pm 0.08	3.1 \pm 0.26	9.0 \pm 0.47	1302 \pm 26	65 \pm 2	1,000 \pm 36	10.1 \pm 0.07	25.0 \pm 0.03
jGCaMP7b	0.6 \pm 0.07	1.2 \pm 0.08	2.9 \pm 0.1	3.5 \pm 0.09	3673 \pm 32	47 \pm 0.1	523 \pm 2	27.4 \pm 0.01	57.8 \pm 0.01
jGCaMP7c	0.3 \pm 0.03	0.8 \pm 0.04	3.9 \pm 0.2	16.7 \pm 0.58	770 \pm 6	49 \pm 0.1	513 \pm 1	9.3 \pm 0.003	21.9 \pm 0.01
jGCaMP7f	0.3 \pm 0.06	0.8 \pm 0.05	2.9 \pm 0.1	7.9 \pm 0.25	1797 \pm 16	46 \pm 0.1	669 \pm 2	13.6 \pm 0.01	28.7 \pm 0.01
jGCaMP7s	0.7 \pm 0.10	2.0 \pm 0.11	4.6 \pm 0.17	4.2 \pm 0.12	1397 \pm 11	42 \pm 0.1	736 \pm 2	24.5 \pm 0.01	57.9 \pm 0.02

617

618

619 **Supplementary Table 4. mNG-GECO1 comparison with GCaMP6s in larval zebrafish 6**
620 **dpf.** Mean values were calculated for the total number of cells (ROI's) across six FOV's in five
621 independent fish. Mean \pm s.e.m. are presented. For max $\Delta F/F_0$, the maximum $\Delta F/F_0$ from each
622 cell is used. For baseline brightness, the raw intensity of the indicator under the same set of
623 imaging conditions is used. For half decay time, 17 and 19 represented cells were used for
624 mNG-GECO1 and GCaMP6s, respectively. The difference in max $\Delta F/F_0$ for the two indicators is
625 significant (Kolmogorov-Smirnov statistic = 0.218, p-value = 1.79×10^{-21}). The difference in
626 baseline brightness for the two indicators is significant (Kolmogorov-Smirnov statistic = 0.100, p-
627 value $\approx 7.31 \times 10^{-5}$). The difference in half decay time for the two indicators is significant
628 (Kolmogorov-Smirnov statistic = 0.666, p-value $\approx 3.00 \times 10^{-4}$).

Protein	# of biological replicates	# of total field of views (FOV)	# of total cells (N)	Max $\Delta F/F_0$	Baseline Brightness ($\times 1000$) (AU)	Signal to noise ratio (SNR)	Half decay time (s^{-1}) (n)
mNG-GECO1	5	6	834	3.09 ± 0.08	0.95 ± 0.03	6.63 ± 0.07	1.98 \pm 0.12 (17)
GCaMP6s	5	6	1280	4.56 ± 0.11	1.41 ± 0.05	5.25 ± 0.04	3.00 \pm 0.12 (19)



629

630 **Supplementary Figure 1 Overview of mNG-GECO1 development**

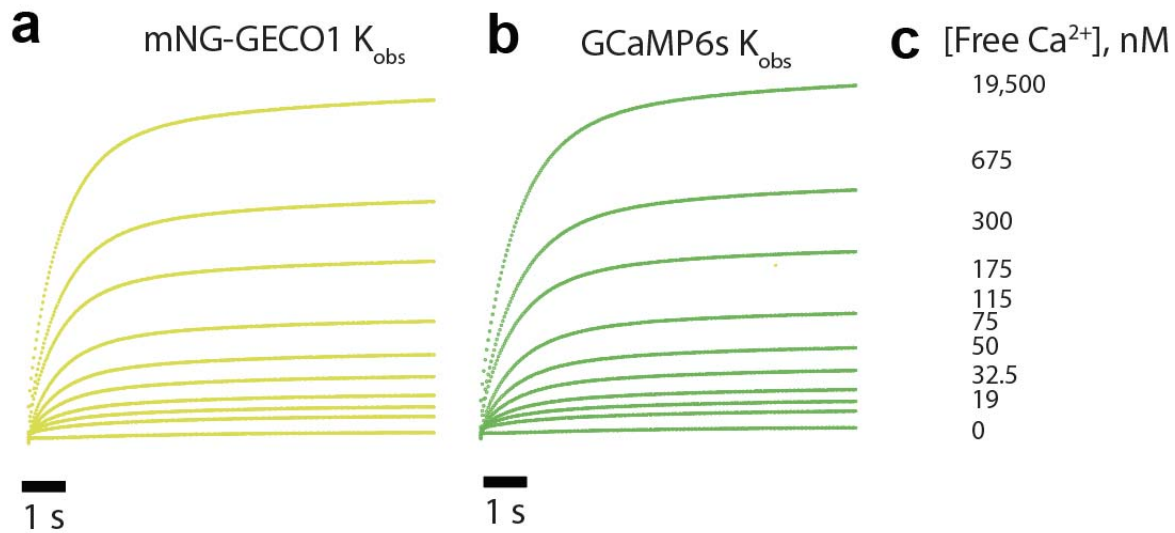
631 Lineage of mNG-GECO variants starting from initial insertion of Ca²⁺ sensing domain into mNG,
632 and ending with the final mNG-GECO1 variant.

		20		40		60	
mNG-GECO0.1	MVSKGEEDNM	ASLPATHELH	IFGSI	INGVDF	DMVGQGTGNP	NDGYEELNLK	STKGDLOQFSP 60
mNG-GECO0.2	MVSKGEEDNM	ASLPATHELH	IFGSI	INGVDF	DMVGQGTGNP	NDGYEELNLK	STKGDLOQFSP 60
mNG-GECO0.7	MVSKGEEDNM	ASLPATHELH	IFGSI	INGVDF	DMVGQGTGNP	NDGYEELNLK	STKGDLOQFSP 60
mNG-GECO0.9	MVSKGEEDNM	ASLPATHELH	IFGSI	INGVDF	DMVGQGTGNP	NDGYEELNLK	STKGDLOQFSP 60
mNG-GECO0.9.1	MVSKGEEDNM	ASLPATHELH	IFGSI	INGVDF	DMVGQGTGNP	NDGYEELNLK	STKGDLOQFSP 60
mNG-GECO1	MVSKGEEDNM	ASLPATHELH	IFGSI	INGVDF	DMVGQGTGNP	NDGYEELNLK	STKGDLOQFSP 60
		80		100		120	
mNG-GECO0.1	WILVPHI	GYG	FHQYLPYPD	G	MSPFQAAMVD	GSGYQVHRTM	QFEDGASLTV NYRYTYEGSH 120
mNG-GECO0.2	WILVPHI	GYG	FHQYLPYPD	G	MSPFQAAMVD	GSGYQVHRTM	QFEDGASLTV NYRYTYEGSH 120
mNG-GECO0.7	WILVPHI	GYG	FHQYLPYPD	G	MSPFQAAMVD	GSGYQVHRTM	QFEDGASLTV NYRYTYEGSH 120
mNG-GECO0.9	WILVPHI	GYG	FHQYLPYPD	G	MSPFQAAMVD	GSGYQVHRTM	QFEDGASLTV NYRYTYEGSH 120
mNG-GECO0.9.1	WILVPHI	GYG	FHQYLPYPD	G	MSPFQAAMVD	GSGYQVHRTM	QFEDGASLTV NYRYTYEGSH 120
mNG-GECO1	WILVPHI	GYG	FHQYLPYPD	G	MSPFQAAMVD	GSGYQVHRTM	QFEDGASLTV NYRYTYEGSH 120
		140		160		180	
mNG-GECO0.1	INGEAQVKGT	GFPADGPVMT	NSLTA	TRDQ	LTEEQIAEFK	EAFSLFDKDG	DGTITTKELG 180
mNG-GECO0.2	INGEAQVKGT	GFPADGPVMT	NSLTA	TRDQ	LTEEQIAEFK	EAFSLFDKDG	DGTITTKELG 179
mNG-GECO0.7	INGEAQV	EGT	GFPADGPVMT	NSLTA	TRDQ	LAGEQIAEFK	EAFSLFDKDG DGTITTKELG 179
mNG-GECO0.9	INGEAQV	EGT	GFPADGPVMT	NSITG	TRDQ	LAGEQIAEFK	EAFSLFDKDG DGTITTKELG 179
mNG-GECO0.9.1	INGEAQV	EGT	GFPADGPVMT	NSITG	TRDQ	LAGEQIAEFK	EAFSLFDKDG DGTITTKELG 179
mNG-GECO1	INGEAQV	EGT	GFPADGPVMT	NSITG	TRDQ	LAEEQIAEFK	EAFSLFDKDG DGTITTKELG 179
		200		220		240	
mNG-GECO0.1	TVLRS	LGQNP	TEAELQDMIN	EVDADGDGTF	DFPEFLTMM	RKMNDADSEE	EIREAFRVFD 240
mNG-GECO0.2	TVLRS	LGQNP	TEAELQDMIN	EVDADGDGTF	DFPEFLTMM	RKMNDADSEE	EIREAFRVFD 239
mNG-GECO0.7	CVLRS	LGQNP	TEAELQDMIN	EVDADGDGTF	DFPEFLTMM	RKMNDADSEE	EIREAFRVFD 239
mNG-GECO0.9	CVLRS	LGQNP	TEAELQDMIN	EVDADGDGTF	DFPEFLTMM	RKMNDADSEE	EIREAFRVFD 239
mNG-GECO0.9.1	CVLRS	LGQNP	TEAELQDMIN	EVDADGDGTF	DFPEFLTMM	RKMNDADSEE	EIREAFRVFD 239
mNG-GECO1	CVLRS	LGQNP	TEAELQDMIN	EVDADGG	GGTL	DFPEFLTMM	RKMNDADSEE EIREAFRVFD 239
		260		280		300	
mNG-GECO0.1	KDNGYI	GAA	ELRHVMTDLG	EKL	TDEEVDE	MIRVADIDGD	GQVNYEEFVQ MMTAKGGGGS 300
mNG-GECO0.2	KDNGYI	GAA	ELRHVMTDLG	EKL	TDEEVDE	MIRVADIDGD	GQVNYEEFVQ MMTAKGGGGS 299
mNG-GECO0.7	KDNGYI	GAA	ELRHVMTDLG	EKL	PK	KEVDE	MIRVADIDGD GQVNYEEFVQ MMTGKGGGGS 299
mNG-GECO0.9	KDNGYI	GAA	ELRHVMTDLG	EKL	PK	KEVDE	MIRVADIDGD GQVNYEEFVQ MMTGKGGGGS 299
mNG-GECO0.9.1	KDNGYI	GAA	ELRHVMTDLG	EKL	PK	KEVDE	MIRVADIDGD GQVNYEEFVQ MMTGKGGGGS 299
mNG-GECO1	KDNGYI	GAA	ELRHVMTDLG	EKL	F	DSEVDE	MIRVADIDGD GQVNYEEFVQ MMTGKGGGGS 299
		320		340		360	
mNG-GECO0.1	VDSSRRKWNK	AGHAVRAIGR	LSSD	WCRS	KK	TYPNDKTIIS	TFKWSYTTGN GKRYRSTART 360
mNG-GECO0.2	VDSSRRKWNK	AGHAVRAIGR	LSSD	WCRS	KK	TYPNDKTIIS	TFKWSYTTGN GKRYRSTART 359
mNG-GECO0.7	VDSSRRKWNK	AGHAVRAIGR	LSSD	WCRS	KK	TYPNDKTIIS	TFKWSYTTGN GKRYRSTART 359
mNG-GECO0.9	VDSSRRKWNK	AGHAVRAIGR	LSSD	WCRS	KK	TYPNDKTIIS	TFKWSYTTGN GKRYRSTART 359
mNG-GECO0.9.1	VDSSRRKWNK	AGHAVRAIGR	LSSD	W	NR	RS	KK TYPNDKTIIS TFKWSYTTGN GKRYRSTART 359
mNG-GECO1	VDSSRRKWNK	AGHAVRAIGR	LSSD	W	NR	RS	KK TYPNDKTIIS TFKWSYITGN GKRYRSTART 359
		360		400			
mNG-GECO0.1	TYTFAK	PMAA	NYLKNQPMYV	FRKTELKHSK	TELNFKEWQK	AFTDVMGMDE	LYK 413
mNG-GECO0.2	TYTFAK	PMAA	NYLKNQPMYV	FRKTELKHSK	TELNFKEWQK	AFTDVMGMDE	LYK 412
mNG-GECO0.7	TYTFAK	PMAA	NYLKNQPMYV	FRKTELKHSK	TELNFKEWQK	AFTDVMGMDE	LYK 412
mNG-GECO0.9	TYTFAK	PMAA	NYLKNQPMYV	FRKTELKHSK	TELNFKEWQK	AFTDVMGMDE	LYK 412
mNG-GECO0.9.1	TYTFAK	PMAA	NYLKNQPMYV	FRKTELKHSK	TELNFKEWQK	AFTDVMGMDE	LYK 412
mNG-GECO1	TYTFAK	PMAA	NYLKNQPMYV	FRKTELKHSK	TELNFKEWQK	AFTDVMGMDE	LYK 412

633

634 **Supplementary Figure 2 Sequence alignment of mNG-GECO variants**

635 Alignment of mNG-GECO variants 0.2, 0.7, 0.9, 0.9.1, and 1. Similar to the topological
636 representation in **Fig. 1a**, mNG barrel (yellow), CaM (light blue), RS20 (green), linker
637 regions (black), mutations (red), and the chromophore forming residues (black box over
638 “GYG”). Also highlighted are the two residues that flank the insertion site (residue 136 of
639 mNG in purple and residue 139 in magenta; numbering as in PDB ID 5LTR), which are
640 shown as circles in both the protein structure and gene schematic in **Fig. 1a**.



641

642 **Supplementary Figure 3** K_{on} , (observed) traces of mNG-GECO1 and GCaMP6s purified
643 protein using Photophysics SX-20 Stopped-flow. Each protein buffered in 30 mM MOPS, 100
644 mM KCl, 50 μ M EGTA is rapidly mixed at 1:1 ratio with varying concentrations of Ca^{2+} produced
645 by reciprocal dilutions of 10 mM EGTA and 10 mM CaEGTA. **a** mNG-GECO1 change in
646 fluorescence over time as Ca^{2+} is rapidly mixed. **b** GCaMP6s change in fluorescence over time
647 as Ca^{2+} is rapidly mixed. **c** Final free- Ca^{2+} concentrations produced after reciprocal dilutions.
648 mNG-GECO1 and GCaMP6s fit with a double exponential curve due to a slow rate limiting step
649 likely caused by the conformational change of the proteins upon binding to Ca^{2+} . Both sensors
650 have a similar $t_{1/2}$ for physiologically relevant Ca^{2+} concentrations.

651

652

653

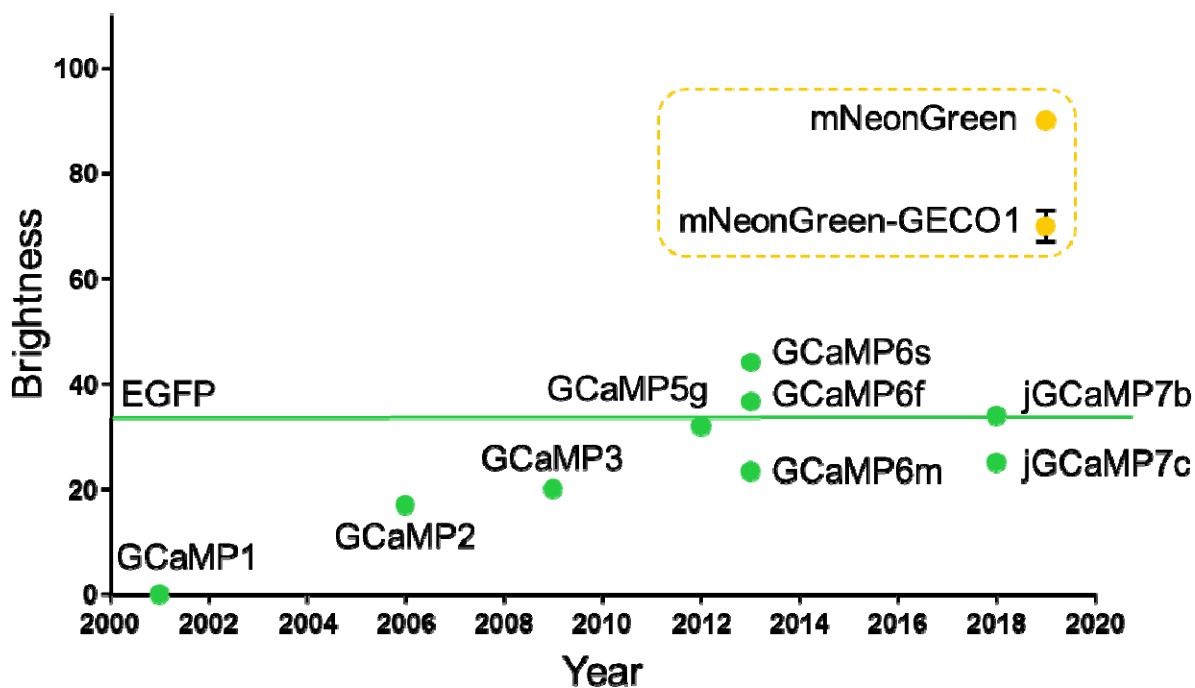
654

655

656

657

658



659

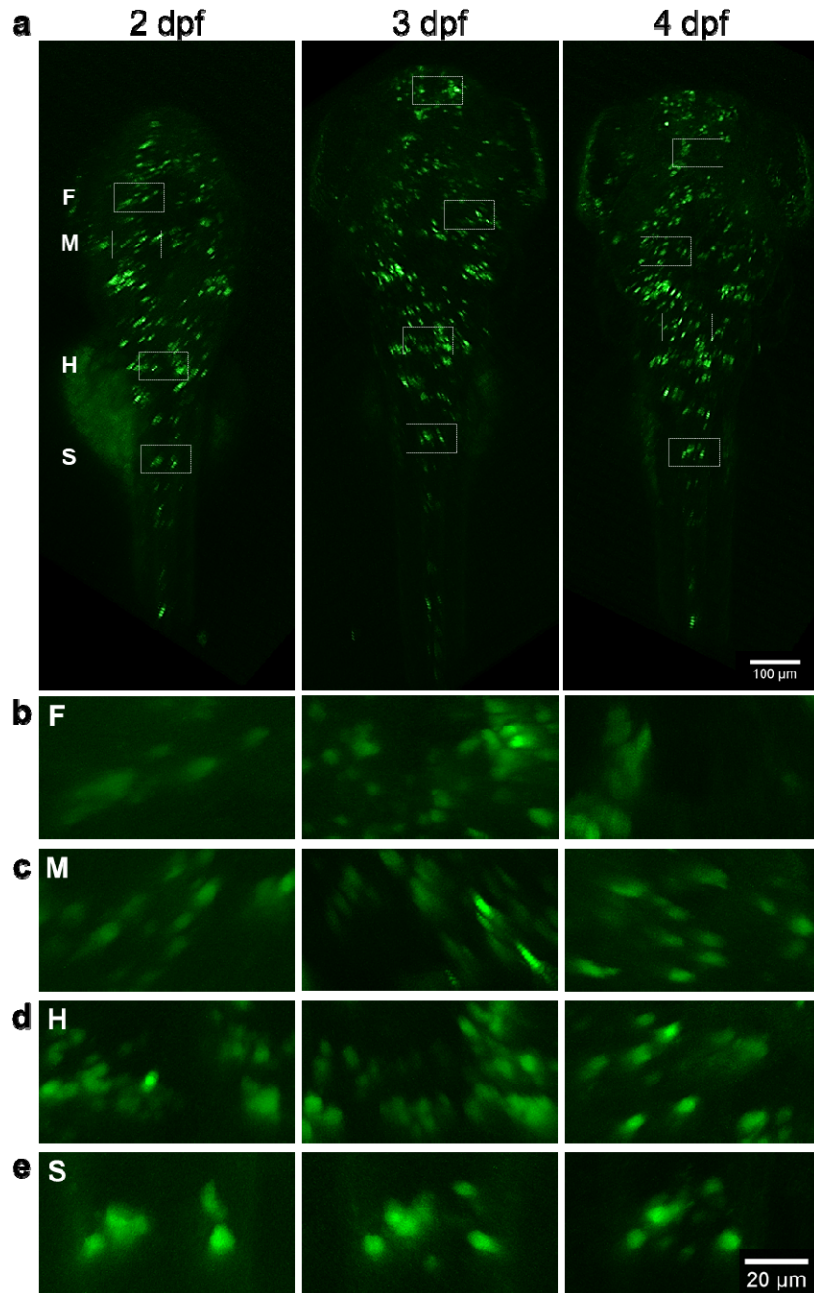
660 **Supplementary Figure 4** *In vitro* brightness comparison of mNG-GECO1 to GCaMP series

661 1P purified protein brightness of first generation mNG-GECO1 compared to the GCaMP series

662 of Ca²⁺ indicators. mNG-GECO1 is substantially brighter *in vitro* than the highly-engineered

663 GCaMP series, which is roughly as bright as its own scaffold, EGFP.

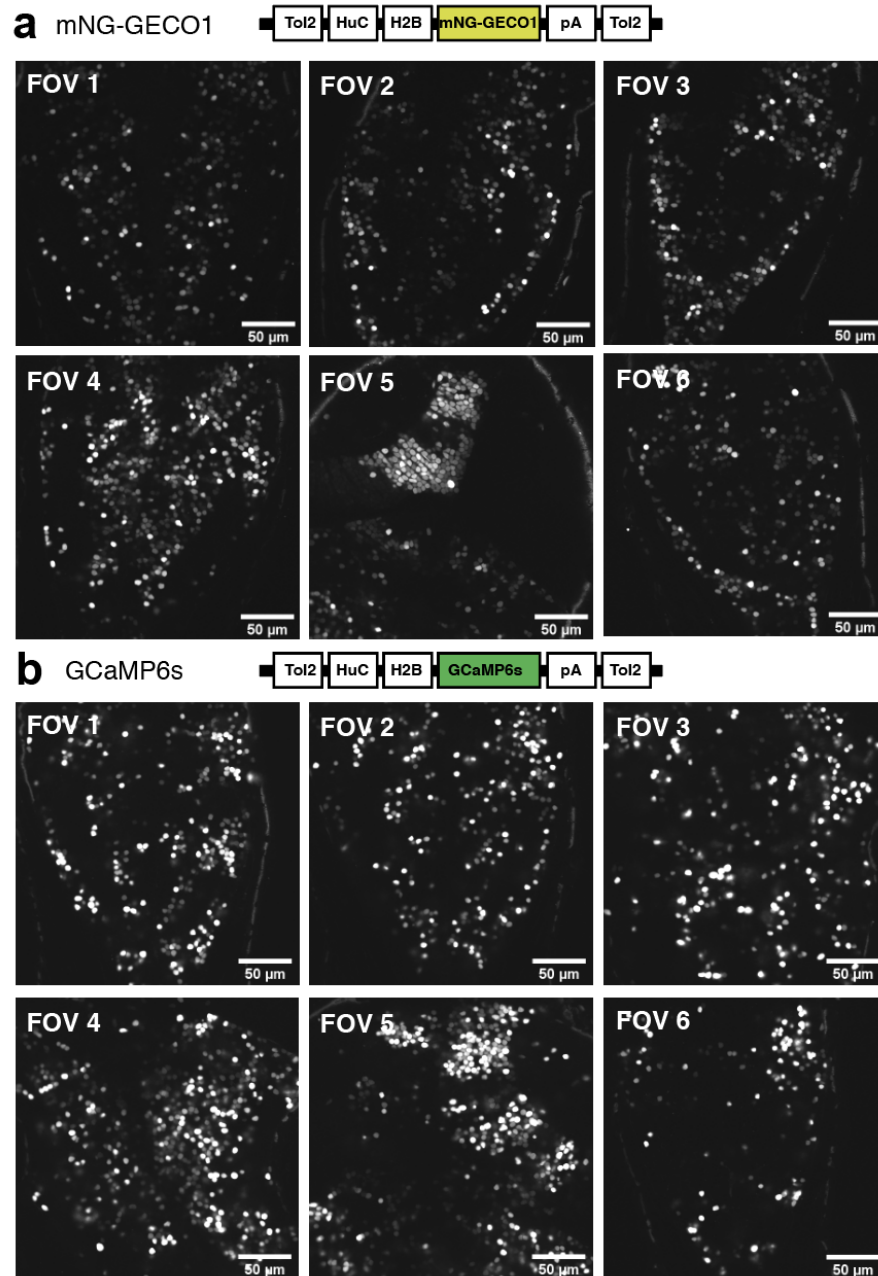
664



665

666 **Supplementary Figure 5 mNG-GECO1 expression profile in zebrafish larvae.** Transient
667 expression of mNG-GECO1 in Tg[elavl3:mNG-GECO1] zebrafish at 2, 3 and 4 days post-
668 fertilization. **a** Dorsal view of confocal z-projections obtained from the whole larvae. Small
669 dashed squares mark areas that have been enlarged and presented in b-e. **b-e** Shows areas in
670 the forebrain (F), midbrain (M), hindbrain (H) and spine (S). Scale bars are 100 μm in A and 20
671 μm in b-e as shown bottom right in e.

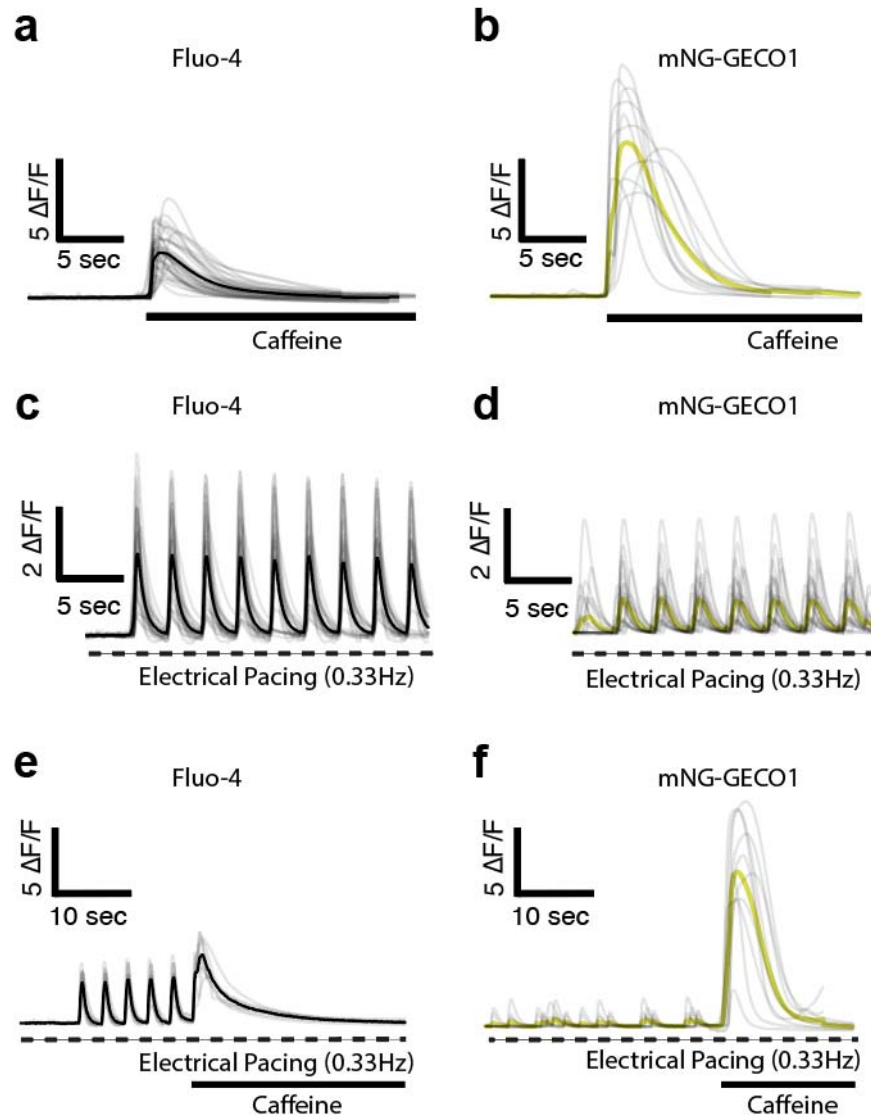
672



673

674 **Supplementary Figure 6 mNG-GECO1 and GCaMP6s field of views (FOV) in zebrafish**
675 **larvae used for quantification.** Transient expression of mNG-GECO1 and GCaMP6s in
676 zebrafish at 6 days post-fertilization. Each FOV image is an average intensity of a 5 minute
677 recording encoding 900 frames. The relative fluorescence intensity is to-scale between the two
678 sensors. **a** FOVs from larvae expressing mNG-GECO1. **b** FOVs from larvae expressing
679 GCaMP6s. Scale bar is 50 μm for all images.

680



681

682 **Supplementary Figure 7** Comparison of Fluo-4 Ca²⁺ dye and mNG-GECO1 in human iPSC-
683 derived cardiomyocytes. **a, b** Single cell Ca²⁺ transient traces from iPSC-CM's loaded with the
684 Fluo-4 Ca²⁺ dye (n = 38 regions of interests [ROI's]) or mNG-GECO1 (n=11 ROI's), respectively.
685 Ca²⁺ transients were evoked using 20 mM caffeine. **c, d** Ca²⁺ transients evoked by electrical
686 pacing were recorded with the Fluo-4 Ca²⁺ dye (n = 25 ROI's) or mNG-GECO1 (n = 22 ROI's),
687 respectively. Cells were stimulated electrically at 0.33 Hz and imaged at 10 Hz frame rate. **e, f**
688 Ca²⁺ transients evoked by electrical pacing (0.33 Hz) and caffeine treatment (10 mM) were
689 recorded at 10 Hz with the Fluo-4 Ca²⁺ dye (n = 8 ROI's) or mNG-GECO1 (n = 8 ROI's),
690 respectively.